

**Polymorphic Phase Dependent Optical and Electrical Properties of
Diketopyrrolopyrrole based Small Molecule**

Shabi Thankaraj Salammal[†], Zhongqiang Zhang[†], Jiehuan Chen[†], Basab Chattopadhyay[‡], Jiake Wu[†], Lei Fu[†], Congcheng Fan[†] and Hongzheng Chen^{†*}

[†] *State Key Laboratory of Silicon Materials, MOE Key Laboratory of Macromolecular Synthesis and Functionalization, Department of Polymer Science and Engineering, Zhejiang University, 38 Zheda Road, Hangzhou 310027, P.R.China.*

[‡] *Universite Libre de Bruxelles (ULB), Faculte des Sciences, Laboratoire Chimie des Polymeres, CP 206/1, Boulevard du Triomphe,1050 Bruxelles, Belgique.*

* *Corresponding Author: hzchen@zju.edu.cn*

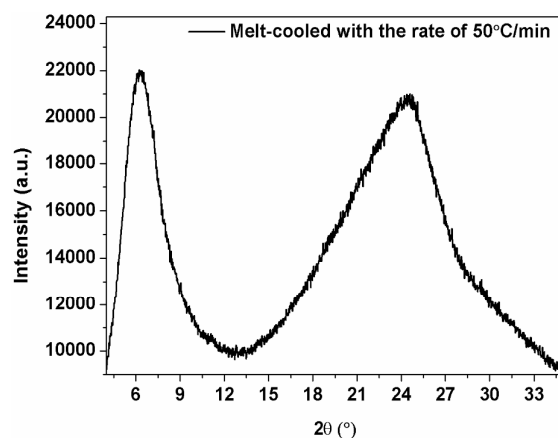


Figure S1. XRD powder pattern of DPP-(CF)₂ melt-cooled with the rate of 50 °C/min.

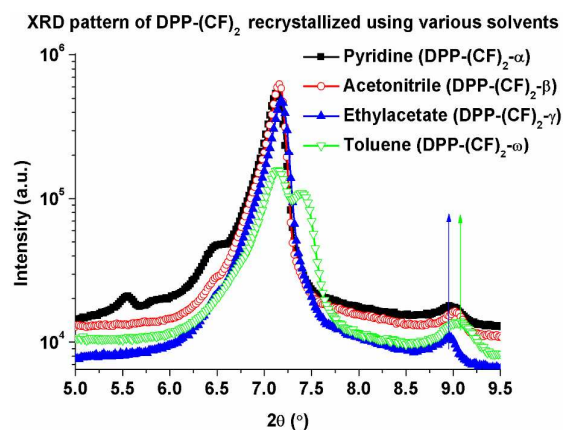


Figure S2. X-ray powder patterns of DPP-(CF)₂ recrystallized using various solvents.

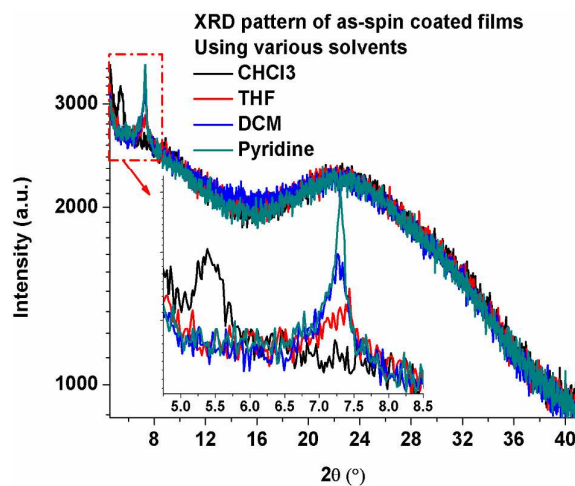


Figure S3. X-ray specular patterns of DPP-(CF)₂ thin films spin coated using various solvents on PEDOT:PSS coated SiO₂ substrate.

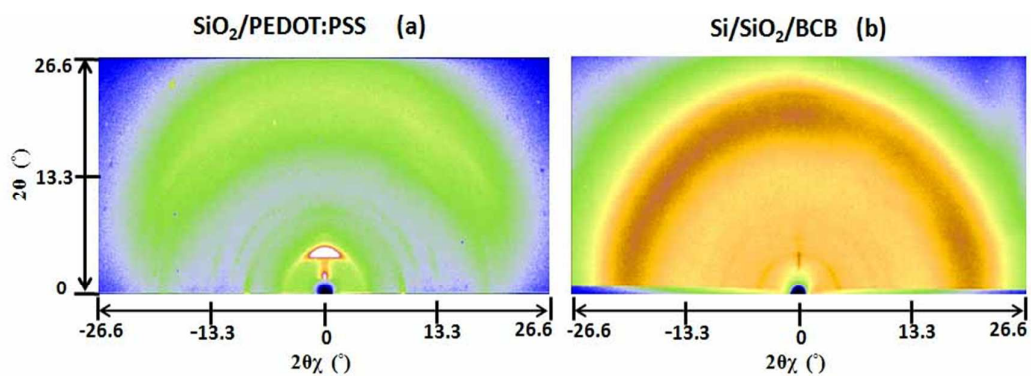


Figure S4. 2D GIXD patterns of DPP-(CF)₂ thin films fabricated on SiO₂/PEDOT:PSS (a) and Si/SiO₂/BCB (b) substrates.

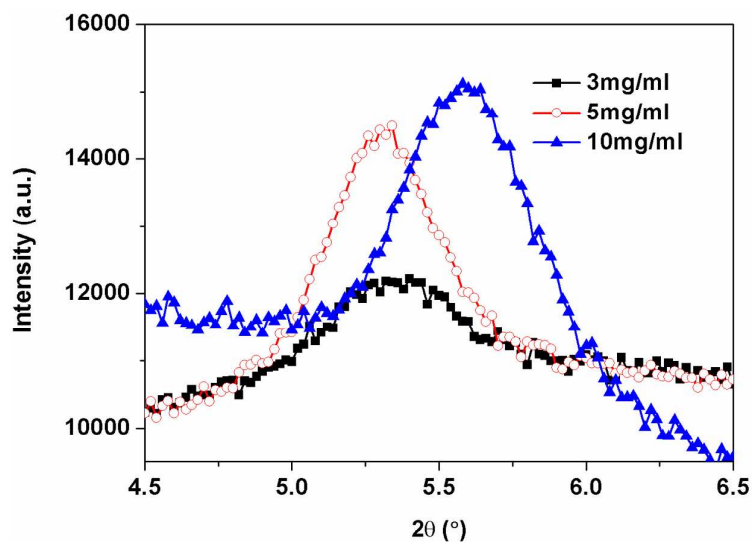


Figure S5. XRD patterns of DPP-(CF)₂ thin films spin coated using various concentrations on PEDOT:PSS coated SiO₂ substrate.

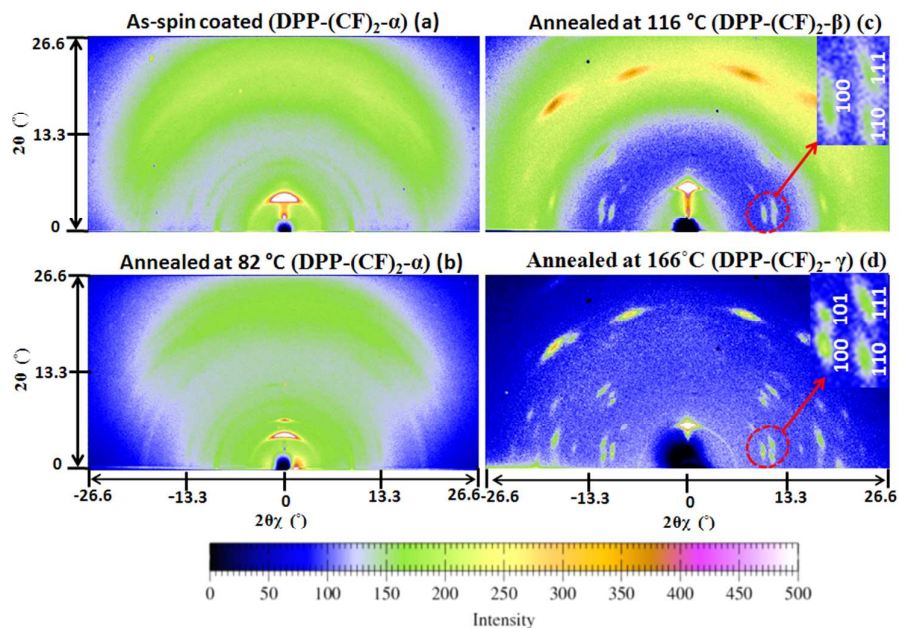


Figure S6. 2D GIXD patterns of DPP-(CF)₂ thin films thermally annealed at various temperatures for the separation of thermally active phases.

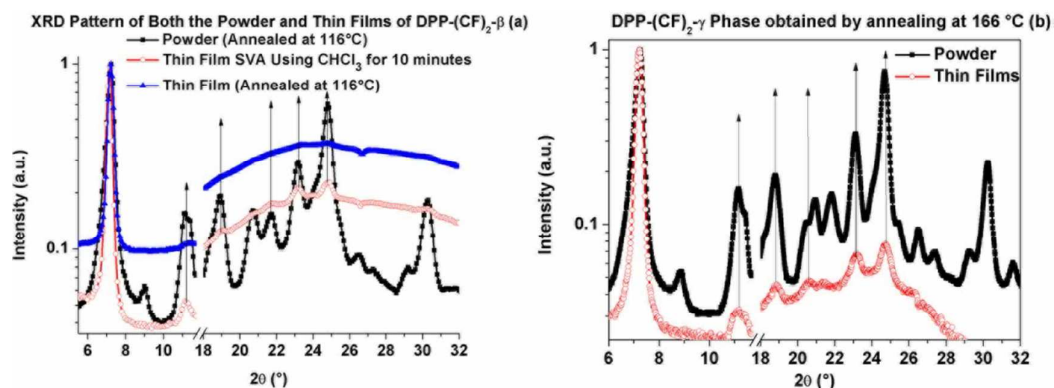


Figure S7. Comparison between the XRD patterns of DPP-(CF)₂- β and DPP-(CF)₂- γ thin films with the corresponding powder patterns obtained by annealing the amorphous DPP-(CF)₂ at 116 and 166 °C..

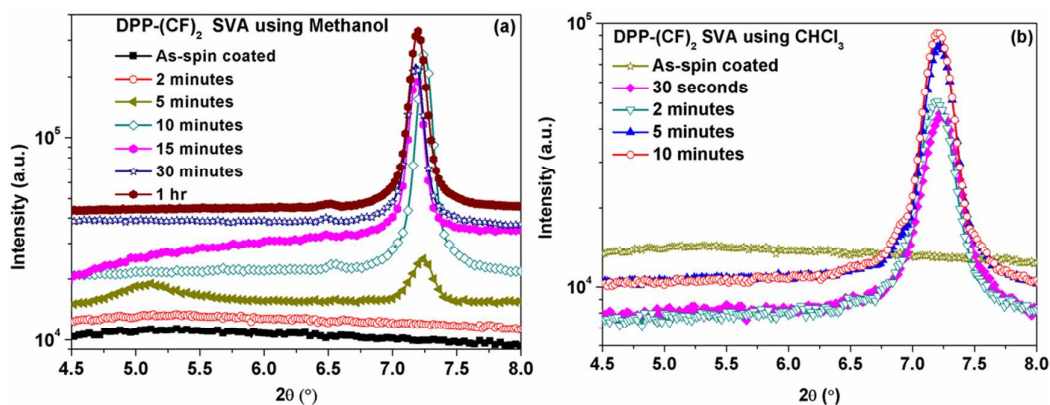


Figure S8. XRD patterns of DPP-(CF)₂ methanol vapor annealed at 27 °C (a) and DPP-(CF)₂ SVA using CHCl₃ (b) for various times.

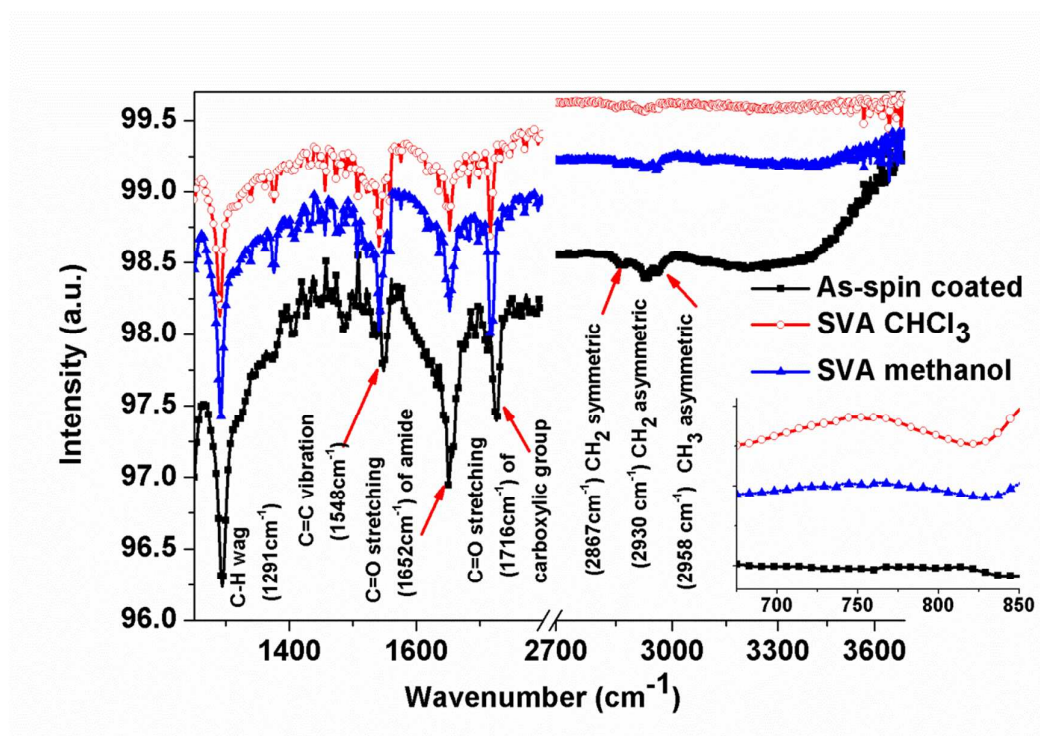


Figure S9. ATR-FTIR spectra of DPP-(CF)₂ SVA using methanol (for 10 minutes) and chloroform (for 10 minutes), inset depicts the spectral range from 675 to 850 cm⁻¹. Absence of any absorption at 750 cm⁻¹ (C - Cl stretching of CHCl₃) and 3337 cm⁻¹ (O-H stretching of methanol) confirms the absence of incorporation of either methanol or chloroform during the solvent vapor annealing, respectively.

AFM Analysis of Various Polymorphs of DPP-(CF)₂

It has been well established in the literature that the SVA tend to dewet the films, which is detrimental for the charge transport due to the augmentation of voids and grain boundaries.¹⁻⁴ So, efforts have been taken to optimize the morphology of the films by optimizing the duration of SVA. AFM height images of four various polymorphs that are patterned on the SiO₂/PEDOT:PSS and Si/SiO₂/BCB substrates are shown on the top and bottom row of Figure S10, respectively. Except DPP-(CF)₂- α , the morphology of other three phases does not vary much with respect to the underlying substrate. On the one hand, the DPP-(CF)₂- α phase patterned on the SiO₂/PEDOT:PSS substrate results in wide platelet shaped crystallites between 100 – 300 nm (Figure S10a), on the other hand, the DPP-(CF)₂- α phase patterned on the Si/SiO₂/BCB substrate results in wavy and ill-defined morphology (Figure S10e). The AFM height images of DPP-(CF)₂- β phase patterned on the SiO₂/PEDOT:PSS and Si/SiO₂/BCB substrates via CHCl₃ vapor annealing are shown in Figure S10b and S10f, respectively. The DPP-(CF)₂- β phase patterned on the SiO₂/PEDOT:PSS substrate results in 200 - 500 nm wide crystallites whereas the DPP-(CF)₂- β phase patterned on the Si/SiO₂/BCB substrate results in the agglomerations of very small crystallites (\approx 20 nm). The size of the agglomerates is found to be nearly equal to the size of the crystallites obtained via CHCl₃ vapor annealing on the SiO₂/PEDOT:PSS substrate. Among the four phases, DPP-(CF)₂- γ results in bigger domains that ranges between 0.3 – 1 μ m (Figure S10c and S10g). The morphology of both the films patterned on both the SiO₂/PEDOT:PSS and Si/SiO₂/BCB substrate is found to be the same. The AFM height images of DPP-(CF)₂- ω phase patterned on the SiO₂/PEDOT:PSS and Si/SiO₂/BCB substrates are shown in Figure S10d and S10h, respectively. As stated earlier, both the DPP-(CF)₂- α and DPP-(CF)₂- ω phases are obtained via methanol vapor annealing for various time (i.e. initial five minutes of methanol vapor annealing supports the crystallization of DPP-(CF)₂- α phase and

further increase in time supports the crystallization of DPP-(CF)₂- ω phase which is fabricated on the SiO₂/PEDOT:PSS substrate). Interestingly, the crystallite size of 5 minutes of methanol vapor annealed film (i.e. DPP-(CF)₂- α) is found to be nearly four times higher than the film undergone 10 minutes of methanol vapor annealing (i.e. DPP-(CF)₂- ω) (Figure S11). This confirms the crystallization of DPP-(CF)₂- ω from the DPP-(CF)₂- α phase via recrystallization process with the initiation of new nucleates.^{3,5} Further increase in SVA duration initiates the unnecessary dewetting of thin films and produces more than 2 μ m long crystallites (Figure S11). Such serious dewetting may be caused by the condensation of methanol vapor on top of the films, which can help the crystallites to migrate and cluster together.^{1,3-4} Independent of the underlying substrate, both the films patterned on the Si/SiO₂/BCB and SiO₂/PEDOT:PSS substrates are noticed to dewet on increasing the duration of methanol vapor annealing (Figure S11 and S12). Since the XRD analysis conducted on the thin films fabricated on the SiO₂/PEDOT:PSS and Si/SiO₂/BCB substrate confirms the complete transformation of DPP-(CF)₂- α to DPP-(CF)₂- ω within the initial 10 minutes and 5 minutes of methanol vapor annealing, respectively, these films are used further for the device analysis. On the contrary to the methanol vapor annealing, CHCl₃ vapor annealing (Figure S13) does not dewet the films on increasing the duration of SVA. Therefore, the films undergone 10 minutes of CHCl₃ vapor annealing are used for both the solar cell and OFET analysis. The dark colored areas present in the films are not corresponding to the voids. Instead they are the depressions present in the films, because depths of those depressions are less than the thicknesses of the films.

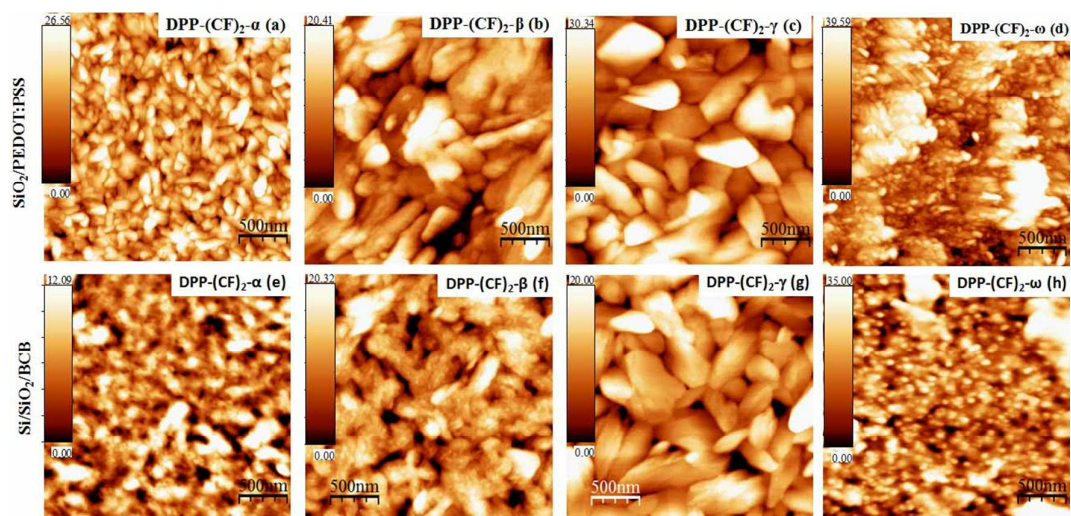


Figure S10. AFM height images of four various polymorphs of DPP-(CF)₂ thin films prepared on the SiO₂/PEDOT:PSS substrates (top row) and Si/SiO₂/BCB substrates (bottom row).

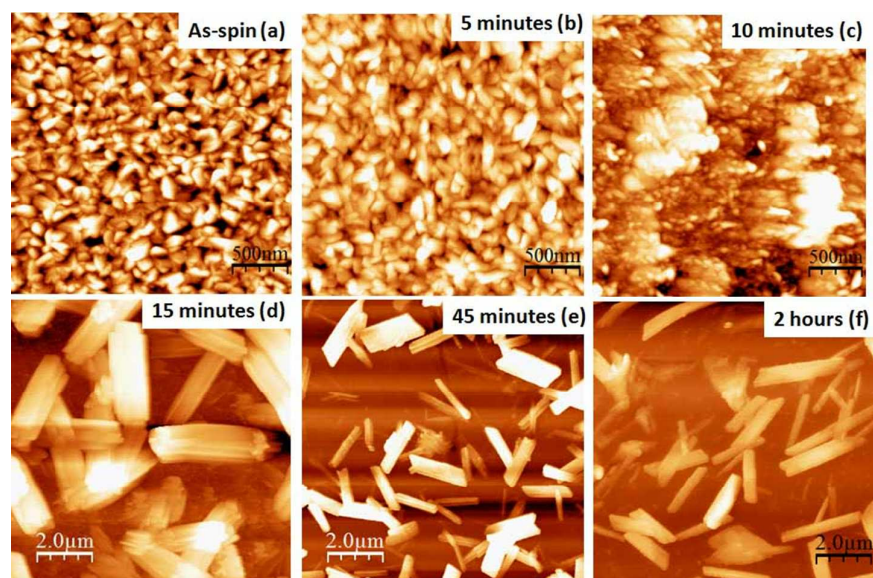


Figure S11. AFM height images of DPP-(CF)₂ thin films fabricated on SiO₂/PEDOT:PSS substrate and undergone methanol vapor annealing at 27 °C for various times.

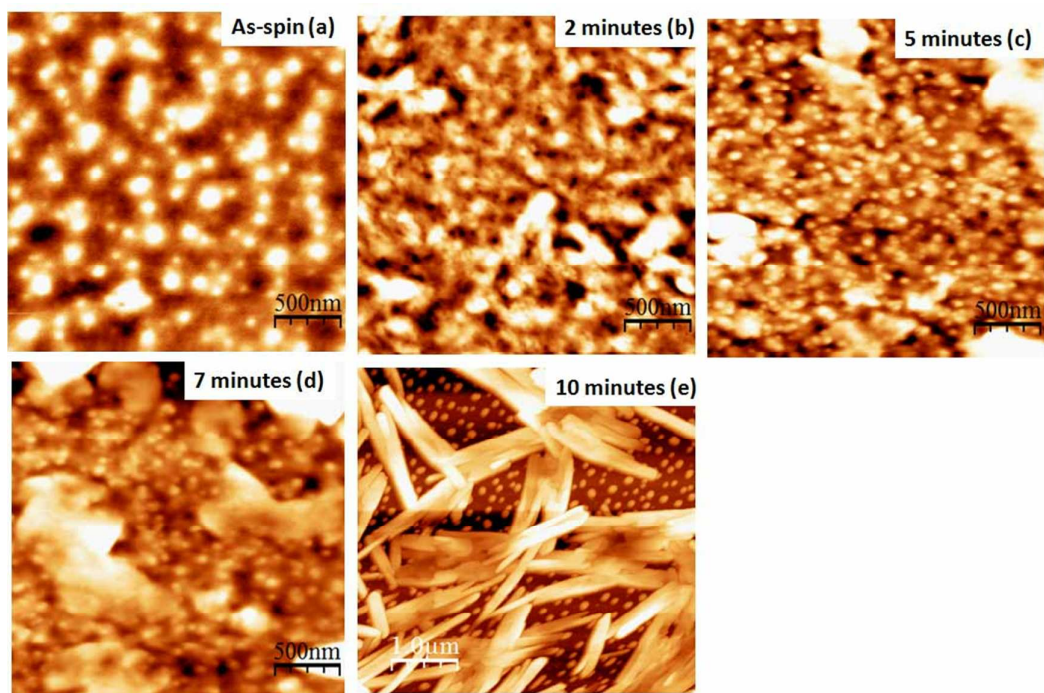


Figure S12. AFM height images of DPP-(CF)₂ thin films fabricated on Si/SiO₂/BCB substrate, which undergone methanol vapor annealing at 27 °C for various times.

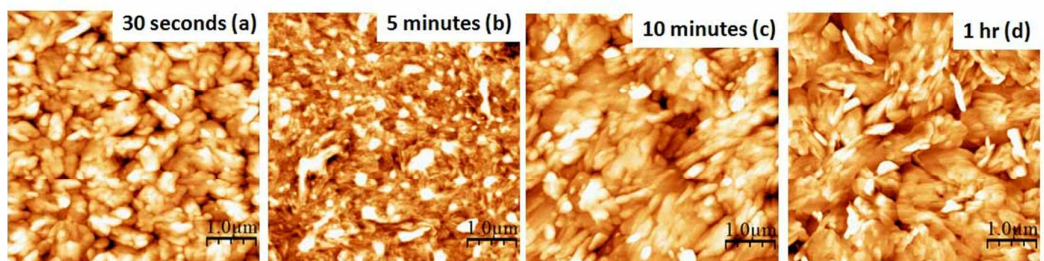


Figure S13. AFM height images of DPP-(CF)₂ thin films SVA using CHCl₃ for various times.

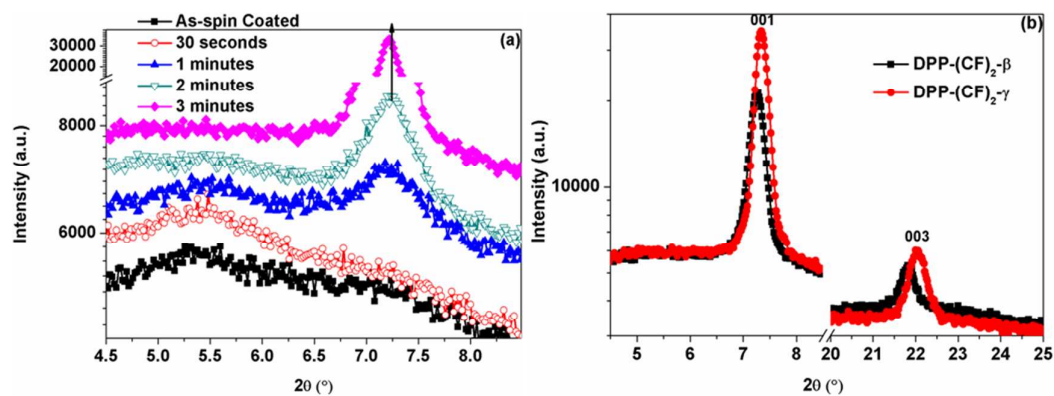


Figure S14. Specular diffraction patterns of DPP-(CF)₂ thin films prepared on the Si/SiO₂/BCB substrate: (a) SVA using methanol for various times and (b) diffraction patterns of DPP-(CF)₂-β (SVA using CHCl₃ for 10 minutes) and DPP-(CF)₂-γ (annealed at 160°C for an hour) phases.

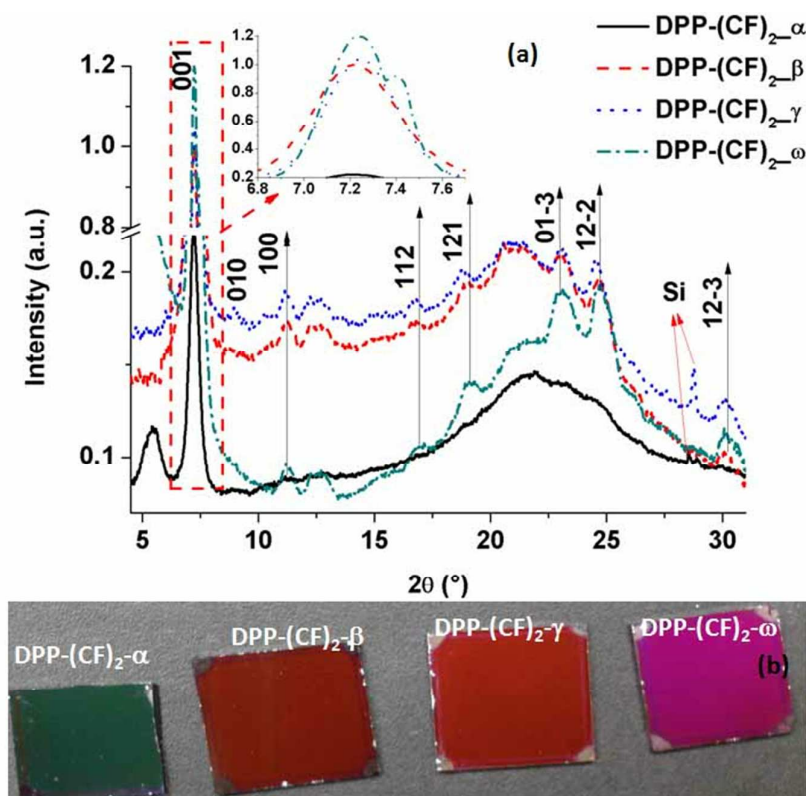


Figure S15. (a) Integrated GIXD patterns of various polymorphs of DPP-(CF)₂ fabricated on the Si/SiO₂/BCB substrate, (b) photograph of the corresponding thin films.

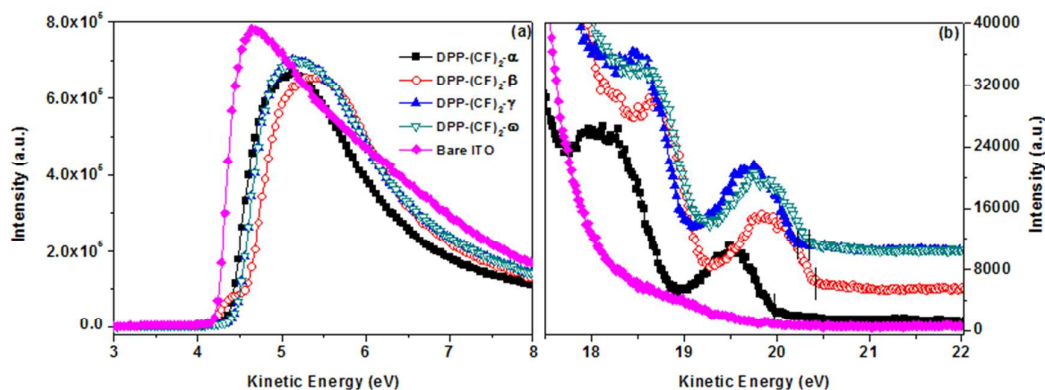


Figure S16. Ultraviolet photoelectron spectra of four different polymorphs of $(\text{DPP-CF})_2$ films and substrate (SiO_2/ITO). (a) and (b) correspond to the low and high kinetic energy part, respectively. The black dotted line in the high kinetic energy part indicates the E_{HOMO} onset.

Fabrication and Testing of Solar Cells

The planar heterojunction (PHJ) solar cells with the following device architecture $\text{ITO}/\text{PEDOT:PSS}/\text{DPP}-(\text{CF})_2/\text{C}_{60}/\text{LiF}/\text{Al}$ were fabricated. $\text{DPP}-(\text{CF})_2$ thin films were first spin coated on the poly(3,4-ethylene dioxythiophene):poly(styrene sulfonate) (PEDOT:PSS, Baytron P AI4083) coated indium tin oxide (ITO) striped ($3 \times 15 \text{ mm}^2$) SiO_2 ($1.5 \times 1.5 \text{ cm}^2$) substrate inside the N_2 filled glove box. Solar cells were fabricated by sequentially depositing $\approx 50 \text{ nm}$ thick C_{60} (acceptor), $\approx 6 \text{ \AA}$ thick lithium fluoride and 80 nm thick aluminum (cathode) on top of the $\text{DPP}-(\text{CF})_2$ thin films, which underwent various postgrowth treatments, via thermal evaporation technique under vacuum. The current density–voltage curve was measured using Keithley 2400 at RT in air (clean room). The photocurrent was measured under a calibrated solar simulator (Abet 300 W) at $100 \text{ mW}/\text{cm}^2$. The mobility of charge carriers (hole mobility) perpendicular to the substrate was measured using the space-charge-limited current (SCLC) technique. To that end, hole only devices were fabricated using the following device architecture $\text{ITO}/\text{PEDOT:PSS}/\text{DPP}-(\text{CF})_2/\text{MoO}_3 (10 \text{ nm})/\text{Al}$. The device characteristics were extracted by modeling the dark current under forward bias using the SCLC expression described by the Mott-Gurney law.⁶

The photovoltaic performances of four various polymorphs are summarized in Table S1. DPP-(CF)₂-β depicts the highest PCE of 0.39% in a PHJ architecture. But the same molecule was reported to have the highest PCE of 5.37% in a bulk heterojunction architecture due to presence of more heterointerface for the exciton dissociation and collection of charge carriers as compared to the PHJ solar cells.⁶⁻⁷ Although the DPP-(CF)₂-ω covers wide solar spectrum (Figure 7 and S17b), which is one of the important characteristics of solar cells, as compared to the other three phases, it results in poor PCE (0.05%). Such decrement in PCE of DPP-(CF)₂-ω could be attributed to the decrement in its V_{OC} of the solar cell due to the upshifting of its HOMO level (Table 3). On the contrary to the DPP-(CF)₂-ω phase, the DPP-(CF)₂-α results in better performance due to increase in V_{OC} of the solar cell, although it has less J_{sc} as compared to the DPP-(CF)₂-ω.⁸⁻⁹

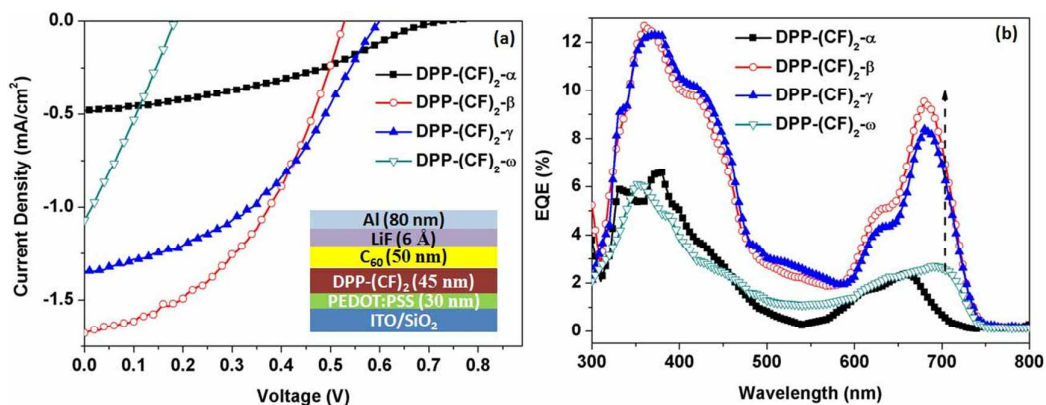


Figure S17. (a) and (b) are the current density-voltage characteristics and EQE curves of various polymorphs of DPP-(CF)₂. Inset of “a” depicts the device structure.

Table S1. Summarizes the solar cell performances of various polymorphs of DPP-(CF)₂.

Polymorphic Phases	V _{oc} (V)	J _{sc} (mA/cm ²)	FF (%)	PCE (%)	Hole mobility perpendicular to the substrate (x 10 ⁻⁵ cm ² /Vs)
DPP-(CF) ₂ -α	0.73	0.48	36	0.13	2.14 ± 0.48
DPP-(CF) ₂ -β	0.53	1.68	43.9	0.39	3.47 ± 0.95
DPP-(CF) ₂ -γ	0.61	-0.86	31.2	0.16	4.32 ± 1.40
DPP-(CF) ₂ -ω	0.18	1.07	27.5	0.05	4.44 ± 1.68

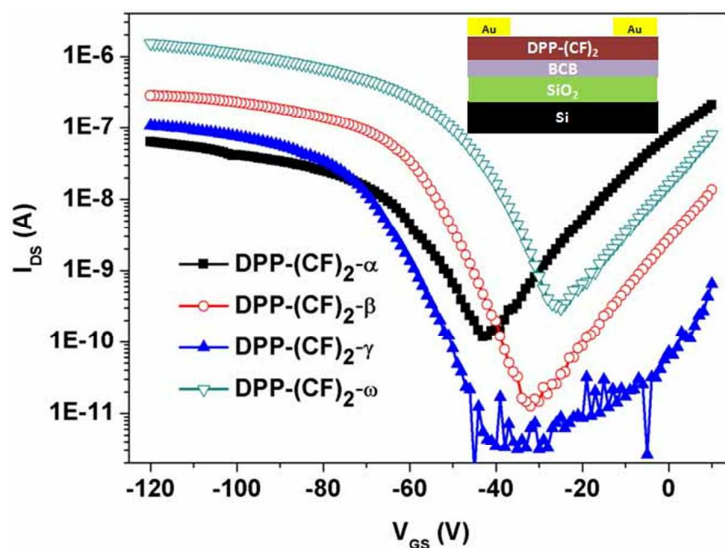


Figure S18. Transfer characteristics of four different polymorphs of DPP-(CF)₂.

Table S2. Summary of the on/off ratio and threshold voltage of various polymorphs of DPP-(CF)₂ based TFT.

Polymorphs	On/Off ratio	Threshold voltage (V)
DPP-(CF) ₂ -α	5.19*10 ⁴	62.8
DPP-(CF) ₂ -β	1.53*10 ⁴	46
DPP-(CF) ₂ -γ	1.6*10 ⁴	39.3
DPP-(CF) ₂ -ω	4*10 ³	28.2

References

1. Ullah Khan, H.; Li, R.; Ren, Y.; Chen, L.; Payne, M. M.; Bhansali, U. S.; Smilgies, D.-M.; Anthony, J. E.; Amassian, A. Solvent Vapor Annealing in the Molecular Regime Drastically Improves Carrier Transport in Small-Molecule Thin-Film Transistors. *ACS Appl. Mater. Interfaces* **2013**, *5*, 2325-2330.

2. Placencia, D.; Wang, W.; Gantz, J.; Jenkins, J. L.; Armstrong, N. R. Highly Photoactive Titanyl Phthalocyanine Polymorphs as Textured Donor Layers in Organic Solar Cells. *J. Phys. Chem. C* **2011**, *115*, 18873-18884.
3. Liu, C.; Minari, T.; Li, Y.; Kumatani, A.; Lee, M. V.; Pan, S. H. A.; Takimiya, K.; Tsukagoshi, K. Direct Formation of Organic Semiconducting Single Crystals by Solvent Vapor Annealing on a Polymer Base Film. *J. Mater. Chem* **2012**, *22*, 8462-8469.
4. Salammal, S. T.; Chen, J.; Ullah, F.; Chen, H. Effects of Material Morphology on the Performance of Organic Electronics. *J. Inorg. Organomet. Polym. Mater* **2014**, *25*, 1-15.
5. Herstein, F. H. On the Mechanism of Some First-Order Enantiotropic Solid-State Phase Transitions: from Simon Through Ubbelohde to Mnyukh. *Acta. Crystallogr. B* **2006**, *62*, 341-383.
6. Fu, L.; Fu, W.; Cheng, P.; Xie, Z.; Fan, C.; Shi, M.; Ling, J.; Hou, J.; Zhan, X.; Chen, H. A Diketopyrrolopyrrole Molecule End-Capped with a Furan-2-Carboxylate Moiety: the Planarity of Molecular Geometry and Photovoltaic Properties. *J. Mater. Chem. A* **2014**, *2*, 6589-6597.
7. Huang, Y.; Kramer, E. J.; Heeger, A. J.; Bazan, G. C. Bulk Heterojunction Solar Cells: Morphology and Performance Relationships. *Chem. Rev* **2014**, *114*, 7006-7043.
8. Walker, B.; Liu, J.; Kim, C.; Welch, G. C.; Park, J. K.; Lin, J.; Zalar, P.; Proctor, C. M.; Seo, J. H.; Bazan, G. C. Optimization of Energy Levels by Molecular Design: Evaluation of Bis-Diketopyrrolopyrrole Molecular Donor Materials for Bulk Heterojunction Solar Cells. *Energ. Environ. Sci* **2013**, *6*, 952-962.
9. Li, W.; Furlan, A.; Roelofs, W. C.; Hendriks, K. H.; van Pruissen, G. W.; Wienk, M. M.; Janssen, R. A., Wide Band Gap Diketopyrrolopyrrole-based Conjugated Polymers Incorporating Biphenyl Units Applied in Polymer Solar Cells. *Chem. Commun* **2014**, *50*, 679-681.